# Adaptive Speed Identification for Vector Control of Induction Motors without Rotational Transducers

Colin Schauder

*Abstract*—**The paper describes a model-reference adaptive system (MRAS) for the estimation of induction motor speed from measured terminal voltages and currents. The estimated speed is used as feedback in a vector control system, thus achieving moderate bandwidth speed control without the use of shaft-mounted transducers. This technique is less complex and more stable than previous MRAS tacholess drives. It has been implemented on a 30-hp laboratory drive, where its effectiveness has been verified.**

## Introduction

MODERN CONTROL techniques for ac motor drives were developed largely as a result of the search for low-cost alternatives to high-performance four-quadrant dc servo drives. In these applications, the use of shaft-mounted tacho generators and resolvers is established practice, and the digital shaft-position encoder used in the most effective vector-control schemes is considered acceptable. Nevertheless, the shaft encoder does present problems. Delicate optical encoders with internal signal-conditioning electronics are widely used. These lower the system reliability, especially in hostile environments, and require careful cabling arrangements with special attention to electrical noise. There are also situations where the positional feedback is extremely difficult to obtain. This is particularly true for the case of linear-motor drives such as for transportation vehicles. Finally, the encoder is a cost factor since the provision of special motor-shaft extensions and encoder-mounting surfaces leads to more expensive machines.

Until recently, the rapid developments in vector control technology have had little impact on "adjustable-speed" ac drives. These are typically simple voltage-source inverters with variable output frequency and are used for applications requiring little dynamic control, such as pumps and fans. It has now become clear that these drives can benefit from the closed-loop current-control techniques that have evolved for use in vector control systems. Current control is readily applicable to existing voltage-source inverters, where it reduces the incidence of over current tripping and improves inverter utilization.

Once the inverter is current controlled, additional controls must be provided to specify the magnitude and slip frequency of the injected current vector and hence regulate the flux and torque of the motor. Motor speed feedback is typically required for outer-loop speed control as well as in the flux and torque control algorithm. This presents a problem in low-performance systems where motor speed transducers are not usually available. This has led to a renewed interest in "tacholess" vector control with the objective of providing an intermediate class of ac drives with enhanced performance and a wider range of applications than "adjustable-speed" drives but about the same cost except for the small additional cost of more sophisticated control algorithms.

The traditional approach to tacholess vector control uses the method of field orientation, either relative to the rotor flux linkage vector or its time derivative [1]. The difficulty in either case lies in determining the instantaneous orientation of the relevant vector. Tamai *et al.* [2] have described an approach in which the field-oriented reference frame is identified by means of a model-reference adaptive system (MRAS). This paper presents an alternative tacholess control method that uses an MRAS to determine the motor speed and thereby establishes vector control of the motor as well as overall speed control. The new MRAS scheme is thought to be less complex and more effective than the previous approach. It has been implemented in a 30-hp drive, which has proved its viability and robust nature.

## Calculation of Motor Speed

Many schemes [3] based on simplified motor models have been devised to sense the speed of the induction motor from measured terminal quantities for control purposes. In order to obtain an accurate dynamic representation of the motor speed, it is necessary to base the calculation on the coupled circuit equations of the motor.

Paper IPCSD 91-144, approved by the Industrial Drives Committee of the IEEE Industry Applications Society for presentation at the 1989 IEEE Industry Applications Society Annual Meeting, San Diego, CA, October 1–5. Manuscript released for publication December 30, 1991.

The author is with the Science and Technology Center, Westinghouse Electric Corporation, Pittsburgh, PA 15235-5098.

IEEE Log Number 9203291.

Since the motor voltages and currents are measured in a stationary frame of reference, it is also convenient to express these equations in the stationary frame:

$$p.\begin{bmatrix}\lambda_d\\ \lambda_q\end{bmatrix} = \frac{L_2}{M}\left[\begin{bmatrix}v_d\\ v_q\end{bmatrix} - \begin{bmatrix}(R_1+\sigma L_1 p.) & 0\\ 0 & (R_1+\sigma L_1 p.)\end{bmatrix}\begin{bmatrix}i_d\\ i_q\end{bmatrix}\right] \quad (1)$$

$$p.\begin{bmatrix}\lambda_d\\ \lambda_q\end{bmatrix} = \begin{bmatrix}(-1/T_2) & (-\omega_r)\\ (\omega_r) & (-1/T_2)\end{bmatrix}\begin{bmatrix}\lambda_d\\ \lambda_q\end{bmatrix} + \frac{M}{T_2}\begin{bmatrix}i_d\\ i_q\end{bmatrix} \quad (2)$$

where $L_{1,2}$ is the stator, rotor self-inductance, $M$ is the mutual inductance, $R_1$ is the stator resistance, $T_2$ is the rotor time constant, $\lambda, i, v$ is the rotor flux, stator current, and stator voltage, respectively, the $d, q$ subscripts denote the $dq$-axis components in the stationary reference frame, $p. = d/dt.$, $\omega_r$ is the rotor electrical angular velocity, and $\sigma$ is the motor leakage coefficient.

Given complete knowledge of the motor parameters, the instantaneous speed $\omega_r$ can be calculated directly from measured voltages and currents on an entirely open-loop basis. First, the angle $\phi$ of the rotor flux vector and its derivative are defined as follows:

$$\phi = \tan^{-1}\left(\frac{\lambda_q}{\lambda_d}\right)$$

$$p.\phi = \frac{\lambda_d(p.\lambda_q) - \lambda_q(p.\lambda_d)}{\left(\lambda_d^2+\lambda_q^2\right)}.$$

Then, substituting for $p.\lambda_d$ and $p.\lambda_q$ in this expression from (2), we obtain

$$p.\phi = \omega_r + \frac{M}{T_2}\left(\frac{i_q\lambda_d - i_d\lambda_q}{\left(\lambda_d^2+\lambda_q^2\right)}\right).$$

This result indicates that the instantaneous angular velocity of the rotor flux vector, as well as its instantaneous slip relative to the rotor, can be obtained from a rotor flux observer based on (1). This process is illustrated in the block diagram of Fig. 1.

This open-loop calculation process requires knowledge of four constants that depend on motor parameters. The parameter sensitivity can be reduced by calculating the slip in a rotating reference frame that is locked to the rotor flux vector. When (2) is transformed to this frame, $\lambda_{q\phi} = p.\lambda_{q\phi} = 0$, and we obtain the following well-known equations:

$$p.\phi - \omega_r = \frac{Mi_{q\phi}}{T_2\lambda_{d\phi}}$$

$$\lambda_{d\phi} = \frac{Mi_{d\phi}}{1+T_2 p.}.$$

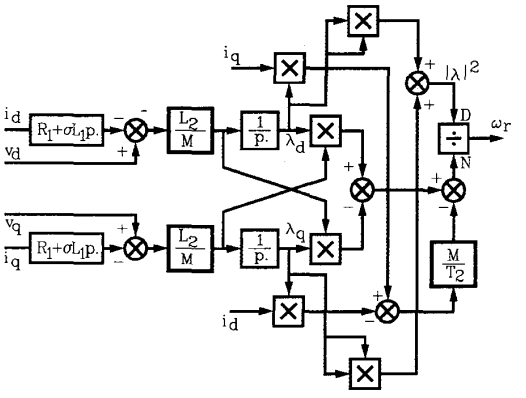


Fig. 1. Open-loop calculation of motor speed.

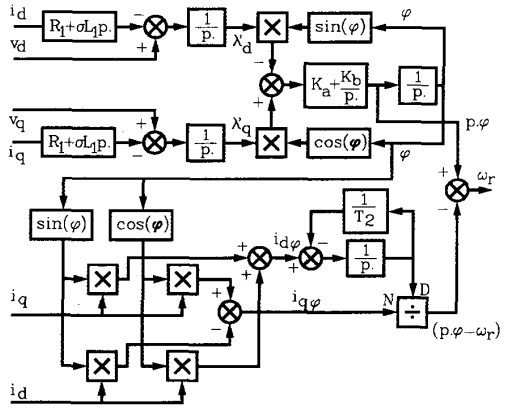


Fig. 2. Speed calculation in the rotor flux vector reference frame.

Fig. 2 illustrates the calculation of motor speed using this method. The angular position of the rotor flux vector $\phi$ is obtained from an observer based on (1) using a vector phase-locked loop with good dynamic response. Notice that the term $L_2/M$ in (1) has been eliminated because this observer is only required to calculate the angle of the flux vector. The current components in flux vector coordinates $i_{d\phi}$ and $i_{q\phi}$ are obtained through a rotating-axis coordinate transformation performed on the measured currents using the angle $\phi$. The calculation of slip frequency from the transformed currents depends only on knowledge of the rotor time constant $T_2$. This approach to the calculation of motor speed thus requires only three constants ($R_1$, $\sigma L_1$, and $T_2$) that depend on motor parameters.

## Speed Identification Using MRAS Techniques

Fig. 3 illustrates an alternative way of calculating the motor speed by means of MRAS techniques. Two independent observers are constructed to estimate the components of the rotor flux vector: one based on (1) and the other based on (2). Since (1) does not involve the quantity $\omega_r$, this observer may be regarded as a reference model of

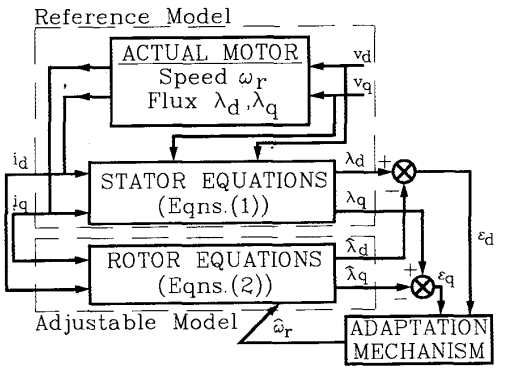


Fig. 3. Structure of MRAS system for speed estimation.

the induction motor, and (2), which does involve $\omega_r$, may be regarded as an adjustable model. The error between the states of the two models is then used to drive a suitable adaptation mechanism that generates the estimate $\hat{\omega}_r$ for the adjustable model. MRAS's of this kind are increasingly being used to identify plant parameters and inaccessible variables. A successful MRAS design can yield the desired values with less computational error than an open-loop calculation and is often simpler to implement.

In designing the adaptation mechanism for a MRAS, it is important to take account of the overall stability of the system and to ensure that the estimated quantity will converge to the desired value with suitable dynamic characteristics. Landau [4] has described practical synthesis techniques for MRAS structures based on the concept of hyperstability. When designed according to these rules, the state error equations of the MRAS are guaranteed to be globally asymptotically stable. Landau's synthesis method leads to candidate structures for the adaptation mechanism but does not establish the dynamics of the convergence process. To study the dynamic response of a particular MRAS, it is always necessary to resort to analysis of the system equations, linearized about a selected operating point.

In general, $\omega_r$ is a variable, and the models are linear time-varying systems. For the purpose of deriving an adaptation mechanism, however, it is valid to initially treat $\omega_r$ as a constant parameter of the reference model. Subtracting (2) for the adjustable model from the corresponding equations for the reference model, we obtain the following state error equations:

$$p.\begin{bmatrix}\varepsilon_d\\ \varepsilon_q\end{bmatrix} = \begin{bmatrix}(-1/T_2) & (-\omega_r)\\ (\omega_r) & (-1/T_2)\end{bmatrix}\begin{bmatrix}\varepsilon_d\\ \varepsilon_q\end{bmatrix} + \begin{bmatrix}-\hat{\lambda}_q\\ \hat{\lambda}_d\end{bmatrix}(\omega_r - \hat{\omega}_r)$$

that is, $p.[\varepsilon] = [A][\varepsilon] - [W]$.

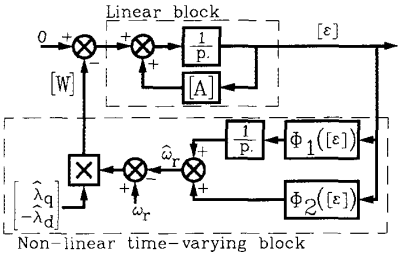


Fig. 4. MRAS representation as a nonlinear feedback system.

Since $\hat{\omega}_r$ is a function of the state error, these equations describe a nonlinear-feedback system as illustrated in Fig. 4. Following Landau, hyperstability is assured, provided that the linear time-invariant forward-path transfer matrix is strictly positive real and that the nonlinear feedback (which includes the adaptation mechanism) satisfies Popov's criterion for hyperstability. It can be shown that the forward path transfer matrix in the present system is indeed strictly positive real (i.e., $[F(j\omega) + F^T(-j\omega)]$ is a strictly positive definite Hermitian matrix, where $F(s) = [sI - A]^{-1}$), but the proof is lengthy and will not be repeated here. Popov's criterion requires a finite negative limit on the input/output inner product of the nonlinear feedback system. Satisfying this criterion leads to a candidate adaptation mechanism as follows:

Let $\hat{\omega}_r = \Phi_2([\epsilon]) + \int_0^t \Phi_1([\epsilon])\, d\tau.$

Popov's criterion requires that

$$\int_0^{t_1} [\epsilon]^T [W]\, dt. \geq -\gamma_0^2 \text{ for all } t_1 \geq 0$$

where $\gamma_0^2$ is a positive constant. Substituting for $[\epsilon]$ and $[W]$ in this inequality and using the definition of $\hat{\omega}_r$, Popov's criterion for the present system becomes

$$\int_0^t \left\{ \left[\epsilon_d \hat{\lambda}_q - \epsilon_q \hat{\lambda}_d\right]\left[\omega_r - \Phi_2([\epsilon]) - \int_0^t \Phi_1([\epsilon])\, d\tau.\right]\right\} dt. \geq -\gamma_0^2.$$

A solution to this inequality can be found through the following well-known relation:

$$\int_0^{t_1} k(p.f(t))f(t)\, dt. \geq -\frac{1}{2}k.f(0)^2,\ k > 0.$$

Using this expression, it can be shown that Popov's inequality is satisfied by the following functions:

$$\Phi_1 = K_2\left(\epsilon_q \hat{\lambda}_d - \epsilon_d \hat{\lambda}_q\right) = K_2\left(\lambda_q \hat{\lambda}_d - \lambda_d \hat{\lambda}_q\right)$$

$$\Phi_2 = K_1\left(\epsilon_q \hat{\lambda}_d - \epsilon_d \hat{\lambda}_q\right) = K_1\left(\lambda_q \hat{\lambda}_d - \lambda_d \hat{\lambda}_q\right).$$

Fig. 5 shows the block diagram of the speed identification MRAS based on this adaptation mechanism. Notice that the factors $L_2/M$ in (1) and $M/T_2$ in (2) have conveniently been incorporated into the adaptation mech-

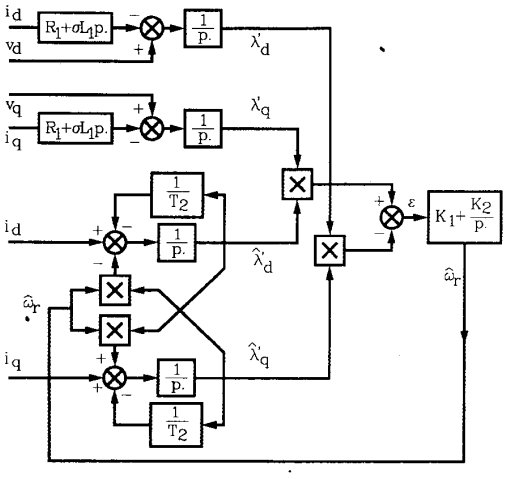


Fig. 5. Block diagram of MRAS speed identification system.

anism gain constants $K_1$ and $K_2$. The outputs of the two models thus only represent the rotor flux vector in angle and have been renamed with primed symbols. As in the system of Fig. 2, the only remaining parameters are $R_1$, $\sigma L_1$, and $T_2$. Note that the angular position of the rotor flux vector is not calculated explicitly, and all variables are expressed in the stationary frame of reference so that the input voltages and currents are obtained from measurements through constant gain terms only.

The MRAS of Fig. 5 can be interpreted as a vector phase-locked loop in which the output flux vector from the reference model $(\lambda'_d + j\lambda'_q)$ is the reference vector, and the adjustable model is a vector phase-shifter controlled by $\hat{\omega}_r$. Examination of the adaptation mechanism shows that the error term $\epsilon$ is proportional to the sine of the angle error between the two vector outputs, thus supporting the notion of a phase-locked loop. The influence of $\hat{\omega}_r$ on the phase of $(\hat{\lambda}'_d + j\hat{\lambda}'_q)$ is seen in the steady-state solution of (2), which leads to the following phasor relationship between input current and output flux.

$$\bar{\lambda} = \frac{M(1 - j(\omega_0 - \omega_{r0})T_2)}{\left(1 + (\omega_0 - \omega_{r0})^2 T_2^2\right)} \bar{I}.$$

Relative to a given input current vector with constant angular frequency $\omega_0$, the phase angle of the output flux vector swings monotonically from $-90°$ to $+90°$ as the value of $\omega_{r0}$ is taken from $-\infty$ to $+\infty$. Fig. 6 shows the error function $\epsilon$ calculated for a 30-hp motor under three different load conditions in the steady state, assuming constant rotor flux vector magnitude and correct motor parameter values. The hyperstability synthesis guarantees that the estimated speed will converge to the actual speed from any initial value, and this can be clearly seen from the sense of the error functions in Fig. 6. These functions always maintain the polarity required to drive the estimate $\hat{\omega}_{r0}$ towards the correct value $\omega_{r0}$.

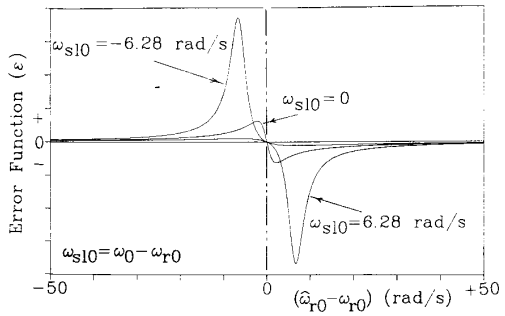


Fig. 6. Steady-state error functions.

*Dynamic Response of MRAS Speed Identification*

In general, the quantities $\hat{\omega}_r$ and $\omega_r$ are time varying, and each may be regarded as an input to a system described by (2). In order to investigate the dynamic response of the MRAS speed identifier, it is necessary to linearize these equations for small deviations about a particular steady-state solution. If this is done in a stationary reference frame, the resulting linear equations will still be time varying; therefore, it is useful to first transform the equations to a reference frame rotating synchronously with the stator current vector. We thus obtain the following equations:

$$p.\begin{bmatrix}\Delta\lambda_{de}\\ \Delta\lambda_{qe}\end{bmatrix} = \begin{bmatrix}\left(\frac{-1}{T_2}\right)(\omega_0 - \omega_{r0}) \\ (\omega_{r0} - \omega_0)\left(\frac{-1}{T_2}\right)\end{bmatrix}\begin{bmatrix}\Delta\lambda_{de}\\ \Delta\lambda_{qe}\end{bmatrix} + \frac{M}{T_2}\begin{bmatrix}\Delta i_{de}\\ \Delta i_{qe}\end{bmatrix} + \begin{bmatrix}-\lambda_{qe0}\\ \lambda_{de0}\end{bmatrix}\Delta\omega_r$$

$$p.\begin{bmatrix}\Delta\hat{\lambda}_{de}\\ \Delta\hat{\lambda}_{qe}\end{bmatrix} = \begin{bmatrix}\left(\frac{-1}{T_2}\right)(\omega_0 - \hat{\omega}_{r0}) \\ (\hat{\omega}_{r0} - \omega_0)\left(\frac{-1}{T_2}\right)\end{bmatrix}\begin{bmatrix}\Delta\hat{\lambda}_{de}\\ \Delta\hat{\lambda}_{qe}\end{bmatrix} + \frac{M}{T_2}\begin{bmatrix}\Delta i_{de}\\ \Delta i_{qe}\end{bmatrix} + \begin{bmatrix}-\hat{\lambda}_{qe0}\\ \hat{\lambda}_{de0}\end{bmatrix}\Delta\hat{\omega}_r.$$

The error function $\epsilon$ has the form of a vector inner product that is independent of the reference frame in which the vectors are expressed. It may thus be represented by the following linearized expression:

$$\Delta\epsilon = \left(\lambda_{qe0}\,\Delta\hat{\lambda}_{de} - \lambda_{de0}\,\Delta\hat{\lambda}_{qe}\right) - \left(\hat{\lambda}_{qe0}\,\Delta\lambda_{de} - \hat{\lambda}_{de0}\,\Delta\lambda_{qe}\right).$$

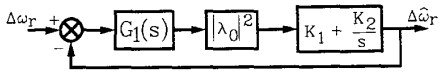


Fig. 7. Block diagram representing MRAS dynamic response.

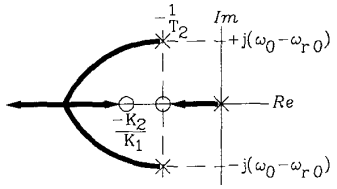


Fig. 8. Sketch of closed-loop root locus (for case $k2/k1 > 1/T2$).

From these equations, we can obtain the transfer function relating $\Delta\omega_r$ to $\Delta\epsilon$ as follows:

$$\left.\frac{\Delta\epsilon}{\Delta\omega_r}\right|_{\Delta\omega_r=0} = \left.\frac{\Delta\epsilon}{\Delta\hat{\omega}_r}\right|_{\Delta\omega_r=0} = \frac{\left(s+\frac{1}{T_2}\right).|\lambda_0|^2}{\left(s+\frac{1}{T_2}\right)^2+(\omega_0-\omega_{r0})^2}$$

$$= G_1(s).|\lambda_0|^2$$

where $|\lambda_0|^2 = (\lambda_{de0}^2 + \lambda_{qe0}^2)$, and we assume that $\lambda_{q0} = \hat{\lambda}_{q0}$, and $\lambda_{d0} = \hat{\lambda}_{d0}$. This allows us to draw a block diagram of the speed identification as shown in Fig. 7. The closed-loop root locus sketch of Fig. 8 illustrates that the achievable bandwidth with which the actual speed can be tracked is limited only by noise considerations.

## Vector Control Using MRAS Speed Estimate

The speed estimate $\hat{\omega}_r$ can be made to track the actual speed very closely and can be used both for speed loop feedback and for orienting the injected stator current vector for torque and flux control. A block diagram illustrating this use of the speed estimate is shown in Fig. 9. An important feature of this system is that, provided the same value of $T_2$ is used in the MRAS adjustable model and in the function blocks of Fig. 9, perfect orientation of the injected current vector is achieved, in theory, even if the value of $T_2$ used is quite wrong. If the MRAS successfully maintains nearly zero error, then the adjustable model accurately replicates the dynamic relationship between the stator current vector and the rotor flux vector that exists in the actual motor. Examination of (2) shows that this is only possible if

$$T_2(\omega - \hat{\omega}_r) = T_{2(\text{actual})}(\omega - \omega_r)$$

where $\omega$ is the instantaneous angular velocity of the stator current vector, that is

$$T_2\,\omega_{sl} = T_{2(\text{actual})}\,\omega_{sl(\text{actual})}.$$

Thus, if $T_2 \neq T_{2(\text{actual})}$, then $\omega_{sl} \neq \omega_{sl(\text{actual})}$, but since only the product $T_2\omega_{sl}$ is used in setting up the injected current vector, this is always done correctly for the actual slip, even under dynamic conditions. Naturally, the error

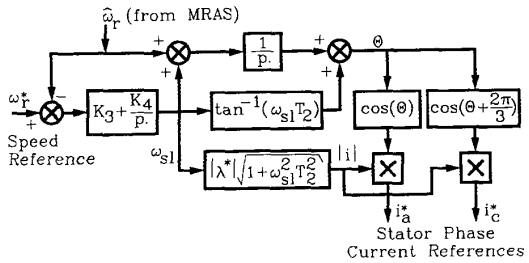


Fig. 9. Vector control system using MRAS speed estimate.

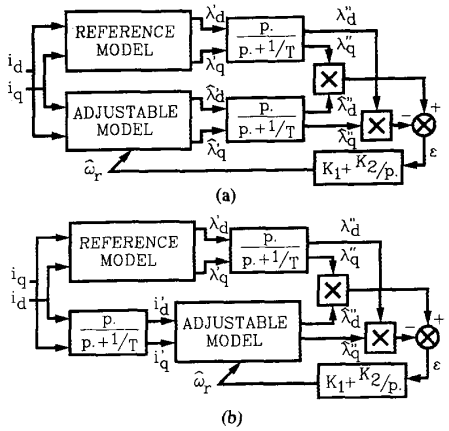


Fig. 10. MRAS's using auxiliary variables.

in the value of $T_2$ will reflect as an error in the speed feedback, which will affect the accuracy of the speed control slightly.

## Practical Considerations

### *Use of Auxiliary Variables*

In practice, the rotor flux observer based on (1) is difficult to implement because of the pure integration of sensed variables that is required. This leads to problems with initial conditions and drift. The MRAS structure has advantages in this regard because the model outputs need not be the actual motor flux components but can be auxiliary variables related to them. Although it is desirable to eliminate the pure integrals, it is also desirable to retain some measure of low-pass filtering in their place. This helps to normalize the model outputs and attenuates the high-frequency components normally found in the motor terminal voltages. Fig. 10 shows two possible ways of modifying the system of Fig. 5 to achieve this objective. In each case, an identical linear transfer matrix is inserted into both the reference and the adjustable model. This block must appear in the output of the reference model since the input cannot be altered, but in the case of the adjustable model, it may appear in either the input or the output as shown.

In Fig. 10(a), the reference and adjustable models have identical structures, but this is no longer a hyperstable system since it does not meet the conditions for hypersta-

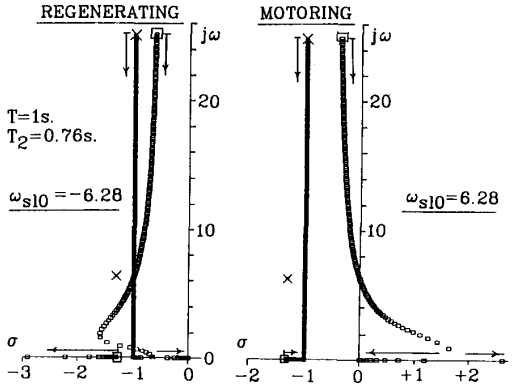


Fig. 11. Pole/zero loci for $G_2(s)$.

bility defined previously. Dynamic analysis of the modified system, following the same lines as before, yields the following transfer function:

$$\frac{\Delta\varepsilon(s)}{\Delta\omega_r(s)} = \frac{\left\{\left(s+\frac{1}{T_2}\right)\left(s^2+\frac{s}{T}+\left(\omega_0^2+\frac{1}{T^2}\right)\right)-\left(\frac{\omega_{sl0}}{T\omega_0}\right)\left(s+\frac{1}{T}\right)s\right\}|\lambda_0''|^2}{\left(\left(s+\frac{1}{T}\right)^2+\omega_0^2\right)\left(\left(s+\frac{1}{T_2}\right)^2+(\omega_{sl0})^2\right)} = G_2(s).|\lambda_0''|^2$$

where $\omega_{sl0} = (\omega_0 - \omega_{r0})$.

Fig. 11 shows the parametric pole/zero locus of this transfer function for a 30-hp motor under two load conditions with $T = 1$ s and $T_2 = 0.76$ s. In each case, the loci start at $\omega_0 = 25.12$ rad/s (4 Hz) and extend to $\omega_0 = 0$ in steps of 0.157 rad/s (0.025 Hz). Notice the complex pole/zero pairs in the region of the excitation frequency. Although the MRAS operates well under most conditions, it is possible to excite these resonant poles through transient changes. A more serious problem is evident in the steady state under extremely low-frequency motoring, where right-plane zeroes indicate probable closed-loop instability. In practice, this MRAS has been found to work well around and through zero frequency, although the speed estimate is not usable if the excitation dwells in the danger zone for more than a few seconds.

In Fig. 10(b), the reference and adjustable models have different mathematical structures, although it can be shown that the system is indeed hyperstable for the special case where $\omega_r$ is a constant. The closed-loop dynamics of this MRAS are identical with those described for the system of Fig. 5. However, when $\omega_r$ is a variable, new dynamics are introduced into the reference path of the speed identification block diagram, as shown in Fig. 12. In effect, the MRAS of Fig. 10(b) removes the excitation-frequency pole/zero pairs from within the high bandwidth identification loop and places them instead in the reference path, where they are less likely to be excited in practice. At very low excitation frequency, the right-plane zeroes now appear in the transfer function between the actual and estimated speeds, and this may be expected to lead to instability of the outer speed-control loop if the

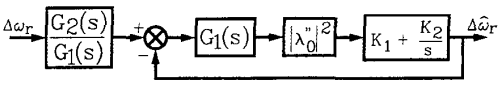


Fig. 12. Speed identification dynamics for Fig. 10(b).

drive is allowed to dwell in this region. The MRAS of Fig. 10(b) is believed to be generally superior to that of Fig. 10(a), and it was therefore used in the experimental system.

Fig. 13 shows a block diagram of this system as implemented in a microcomputer for control of a 30-hp drive. Notice that some functions are performed in analog circuitry external to the computer so that the signals sampled through the A/D interface have limited high-frequency components. The analog circuitry requires amplifiers with extremely low offset voltages to eliminate the need for adjustments. Note the offset-nulling integrators $K_c/p$., which have very low gain and serve to eliminate residual offsets.

*Motor Parameter Sensitivity*

As has been mentioned, the parameter $T_2$ has negligible influence on the operation of the overall MRAS/vector control system. The terms $\sigma L_1$ and $R_1$ influence the accuracy with which the observer based on (1) represents the phase angle of the rotor flux vector. An error in the angle of the reference model output is tracked by the adjustable model with a corresponding error in $\hat{\omega}_r$. This results in the machine operating at a different flux level from that intended, with a consequent change in the maximum torque capability. The effect of an error in $R_1$ is usually quite negligible at high excitation frequency but becomes more serious as the frequency approaches zero. This occurs because the term $R_1\bar{i}/p$. becomes relatively larger as the frequency decreases. In contrast, an error in $\sigma L_1$ has roughly the same effect at all excitation frequencies, where it is zero when the slip frequency is zero and becomes worse under load. It is therefore very important to minimize the error in the value of $\sigma L_1$ used in the reference model.

In the experimental system, the motor parameters are automatically measured when the drive is at rest by means of injected currents that produce stationary or pulsating fields and, hence, do not produce net torque. This subsystem uses a number of MRAS's and is illustrated in Fig. 14. $R_1$ is identified with SW1 closed and with an arbitrary $d$-axis injected dc current. SW1 is then opened, and the value of $\sigma L_1$ is read from an analog MRAS that capitalizes on the high-frequency content of the motor voltage. The $d$-axis current is then pulsed to produce the test

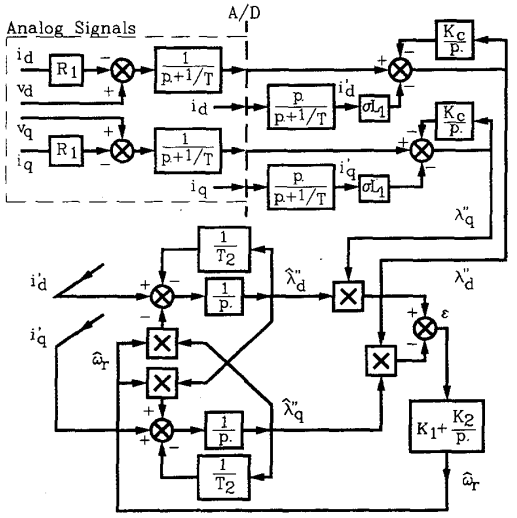


Fig. 13. Microprocessor implementation block diagram.

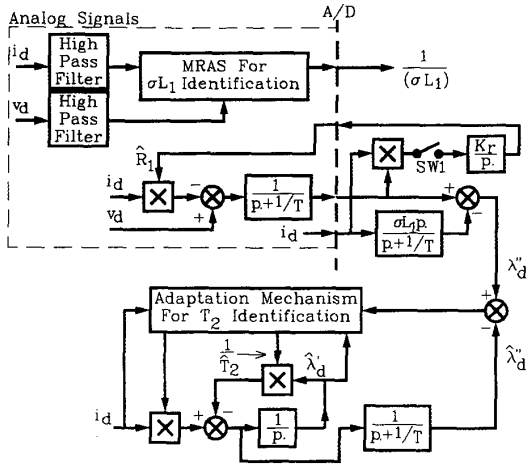


Fig. 14. Adaptive systems for parameter identification.

excitation for the MRAS that identifies $T_2$. The adaptation mechanism for this MRAS is obtained by hyperstability synthesis using (2) with $\omega_r = 0$, and its convergence from an initial zero estimate to the correct final value is illustrated in the oscillogram of Fig. 15.

## Performance of the Experimental System

An experimental drive system was built and tested using the MRAS/vector control technique, which has been described. Both the MRAS of Fig. 13 and the vector control algorithm of Fig. 9 are executed in a 16-b microcomputer that delivers current references to the PWM inverter current-control system. The test machine is a standard 30-hp, 230-V, 60-Hz cage induction motor that is coupled to a dc motor of similar rating. The inertia of the set is, thus, more than twice that of the induction motor alone. A speed measurement signal is available from a dc

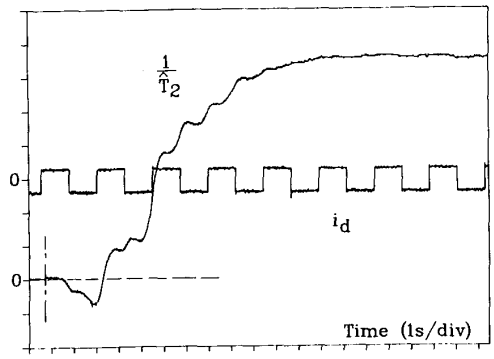


Fig. 15. Measured response of $T_2$ identification.

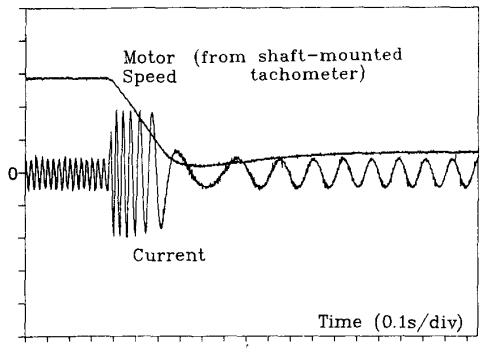


Fig. 16. Measured response of experimental system.

tachogenerator for reference purposes. Motor current feedback signals are obtained using Hall-effect current sensors, and the motor terminal voltages are sensed with resistive voltage dividers followed by differential amplifiers.

Under operating conditions away from zero speed, the performance of the drive is very satisfactory, and speed loop bandwidths of 10 to 15 rad/s are easily obtained. This performance is maintained to quite low speeds (around 2-Hz excitation) and, in fact, is available right through zero speed on a transient basis. However, if the drive is allowed to dwell at zero frequency excitation for more than a few seconds, the amplitude of the MRAS model outputs goes to zero, and speed control is lost. Work is presently underway to determine suitable sequencing techniques that will make this condition acceptable in a practical application. Figs. 16–18 illustrate the dynamic response of the experimental system.

## Conclusion

This work was aimed at developing a low-performance tacholess vector control system that would allow existing "adjustable-speed" drives to benefit from closed-loop current-control techniques. In fact, the performance of the system has exceeded initial expectations and approaches that of vector control systems using shaft position encoders. Despite some limitations in the region of zero-

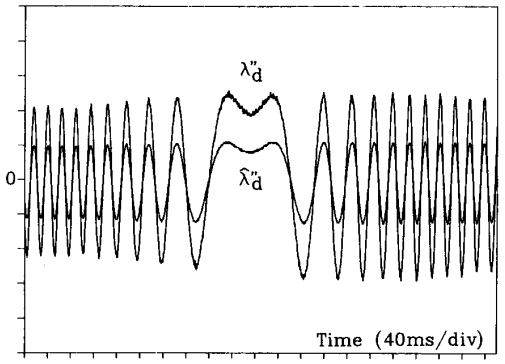


Fig. 17. Model outputs during rapid reversal.

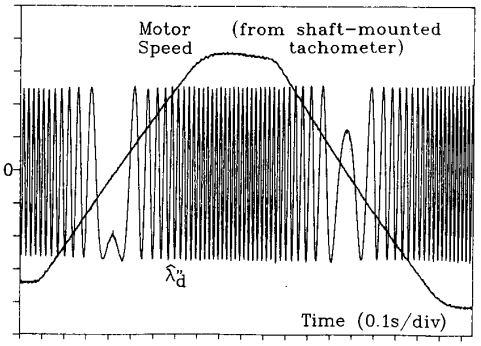


Fig. 18. Measured response of experimental system.

speed operation, it is expected that the MRAS/vector control technique will find practical use in a large number of ac motor drive applications.

## REFERENCES

[1] R. Jotten and G. Maeder, "Control methods for good dynamic performance induction motor drives based on current and voltage as measured quantities," *IEEE Trans. Industry Applications*, vol. IA-19, no. 3, pp. 356–363, 1983.

[2] S. Tamai, H. Sugimoto, and M. Yano, "Speed sensor-less vector control of induction motor applied model reference adaptive system," in *Conf. Rec. IEEE/IAS Ann. Mtg.*, 1985, pp. 613–620.

[3] A. Abbondanti, and M. B. Brennen, "Variable speed induction motor drives use electronic slip calculator based on motor voltages and currents," *IEEE Trans. Industry Applications*, vol. IA-11, no. 5, pp. 483–488, 1975.

[4] Y. D. Landau, *Adaptive Control—The Model Reference Approach*. New York: Marcel Dekker, 1979.

**Colin Schauder** received the B.Sc (Hons.) and Ph.D. degrees in electrical engineering from the University of Cape Town, South Africa, in 1972 and 1978, respectively.

From 1978 to 1983, he was employed by GEC Electrical Projects Ltd. and GEC Industrial Controls, Rugby, Warwickshire, England, where he worked on the development of high-performance ac motor drive systems. Since 1983, he has been with the Westinghouse Electric Corporation at the Science and Technology Center, Pittsburgh, PA, where he is presently an Advisory Engineer in the Power Electronics Department. His work involves the design and development of advanced power conversion systems, including motor drives and static compensators for utility power line applications.